Bioinspired structural heterogeneity directs host remodeling and limits intimal hyperplasia in small-diameter vascular grafts

Marianna Barbuto[1,2,3,4], *Arianna Adamo*[1,5], *Beatrice Di Caccamo*[1,6], *Taro Fujii*[3,4], *Keishi Kohyama*[3,4], *Laura Modica De Mohac*[1], *William D'Angelo*[4], *Tara Richards*[7], *Carlo Mannina*[8], *Amber Wish*[4], *Lance Nicholls*[4], *Salma O. El-Mossier*[4,9], *Seungil Kim*[3,4,10], *George Hussey*[4,9], *Stephen F. Badylak*[3,4,11], *William R. Wagner*[3,11], *Julie A. Phillippi*[3,7], *Antonio D'Amore*[1,3,4,12 *]

1 Ri.MED Cardiovascular Tissue Engineering Laboratory, Ri.MED Foundation, Palermo, Italy

2 Department of Biological, Chemical and Pharmaceutical Sciences and Technologies (STEBICEF), University of Palermo, Palermo, Italy

3 Departments of Bioengineering and Surgery, University of Pittsburgh, Pittsburgh, USA

4 McGowan Institute for Regenerative Medicine, University of Pittsburgh, USA

5 Department of Surgery, Columbia University, New York, USA

6 Polytechnic University of Turin, Turin, Italy

7 Department of Cardiothoracic Surgery, University of Pittsburgh School of Medicine, Pittsburgh, USA

8 Department of Medicine, Mount Sinai Morningside and West, New York, New York, USA

9 Department of Pathology, School of Medicine, University of Pittsburgh, Pittsburgh, USA

10 Biomedical Engineering, Department of Agricultural and Biological Engineering, Mississippi State University, Mississippi State, MS, USA

11 Department of Chemical Engineering, University of Pittsburgh, Pittsburgh, USA

12 Department of Precision Medicine, Surgery and Urgent Care, University of Palermo, Palermo

*Corresponding Author; E-mail: adamore@fondazionerimed.com

Abstract

Small-diameter vascular grafts remain a major unmet clinical need due to their susceptibility to thrombosis, intimal hyperplasia, and poor long-term patency. Here, we introduce a biomimetic three-layered vascular graft (3LVG) designed to recapitulate the functional heterogeneity of native arteries through a structural gradient that guides host cell infiltration and vascular remodeling. The graft integrates an electrospun poly(carbonate-urethane) urea (PCUU) layer, a bioactive decellularized extracellular matrix medial layer, and a porous thermally induced phase separation PCUU layer. The combination of these techniques produced layers with different pore size ranges to preferentially promote either adventitial-derived (ACR) or intimal-derived (ICR) cell recruitment. Implanted as abdominal aortic interposition grafts in rats, ACR grafts showed superior in vivo performance, with 100% patency at 4 and 8 weeks, whereas ICR grafts demonstrated reduced patency associated with anastomotic intimal hyperplasia. ACR grafts also exhibited enhanced endothelialization, greater adventitial cell infiltration, increased collagen deposition, more abundant vasa vasorum formation, and compliance comparable to native vessels at 8 weeks. These findings demonstrate that bioinspired structural heterogeneity can direct host remodeling, reduce maladaptive luminal responses, and improve graft performance. This work identifies structural gradient-driven cell recruitment as a promising design principle for next-generation small-diameter tissue-engineered vascular grafts.

Keywords: Small-diameter vascular graft, functional heterogeneity, biomimicry, engineered tunica.

1. Introduction

Cardiovascular diseases (CVDs) remain the leading cause of mortality globally, with coronary artery disease (CAD) representing the most prevalent and life-threatening condition among them. According to the latest update from the American Heart Association (2024), CAD accounts for 42.6% of all deaths attributed to CVDs in the United States, affecting approximately 20.5 million adults over the age of 20, with a prevalence rate of 7.1% [1]. This alarming burden is compounded by lifestyle-related risk factors such as hypertension, dyslipidemia, diabetes, obesity, smoking, and sedentary behavior [2]. The economic impact is similarly substantial: the direct costs of CAD management already exceed $300 billion annually in the United States alone [3], with projections forecasting a combined direct and indirect cost of nearly $1.1 trillion by 2035 [2].

CAD pathogenesis is intimately linked to atherosclerosis, a progressive and chronic inflammatory disease of the arterial wall. Atherosclerotic lesions develop over time through the luminal accumulation of low-density lipoproteins (LDL), infiltration of monocytes, smooth muscle cell (SMC) migration, and extracellular matrix (ECM) remodeling [4-6]. These processes culminate in the formation of a fibrous cap covering a lipid-rich necrotic core. The rupture or erosion of unstable plaques or "vulnerable plaques" can abruptly occlude coronary arteries, triggering myocardial infarction, stroke, or sudden cardiac death [7]..In late-stage CAD, restoration of myocardial perfusion is critical. The two primary revascularization approaches are percutaneous coronary intervention (PCI) and coronary artery bypass grafting (CABG) [8, 9]. PCI involves balloon angioplasty and stent deployment and is generally preferred in cases of single-, two-, and even selected three-vessel or left main coronary artery disease. Moreover, PCI represents the treatment

of choice in the setting of acute myocardial infarction due to its rapid reperfusion capability and minimally invasive nature. However, CABG remains the standard of care for patients with complex or multivessel disease, particularly when long-term patency and survival [10]are prioritized. Over 400,000 CABG procedures are performed annually in the United States, further underscoring the clinical importance of this surgical remedy [1]. This evolving clinical scenario further highlights the necessity for novel vascular graft substitutes capable of addressing the increasing complexity and extent of coronary artery disease in contemporary CABG candidates [11].

Autologous conduits such as the great saphenous vein (SV), radial arteries (RAs), and the internal thoracic artery (ITA) are most commonly harvested for CABG [12, 13]. Arterial grafts like the ITA offer superior long-term patency rates of 85% at 10 years compared to approximately 60% for venous grafts [13-15]. However, the use of autologous vessels does not come without limitations. Bilateral ITA harvesting increases operative complexity and may compromise sternal and thoracic wall vascularization, thereby increasing the risk of wound healing complications, especially in diabetic, obese, or otherwise high-risk patients. Although the radial artery represents an effective alternative conduit, its availability may still be limited, and long-term performance remains inferior to that of the ITAs in certain clinical settings. Vein grafts are susceptible to intimal hyperplasia, aneurysmal dilation, and accelerated atherosclerosis due to their mechanical inadequacy to function within the arterial circulation [16]. Moreover, anatomical availability is limited, particularly in elderly or comorbid patients. As a result, approximately one-third of patients undergoing CABG may lack suitable autologous graft material [16, 17].

To address this unmet clinical need, synthetic vascular grafts composed of polyethylene terephthalate (PET, Dacron®) or expanded polytetrafluoroethylene (ePTFE, Gore-Tex®) have been investigated [18, 19]. While effective in large-diameter applications (>6 mm), these materials fail in small-diameter settings (<6 mm), especially in coronary or below-knee bypass procedures [10]. Patency rates for small diameter ePTFE grafts remain suboptimal, with frequent failure due to thrombosis, compliance mismatch, low endothelialization, and intimal hyperplasia [10, 20-22]. These challenges highlight the urgent need for alternative strategies capable of matching the mechanical and biological performance of native small diameter vessels.

Over the past two decades, tissue engineering has emerged as a promising approach for developing small-diameter vascular grafts (TEVGs) with the potential for *in situ* regeneration. The general goal of TEVGs is to provide mechanically robust, bioactive scaffolds that support host cell infiltration, ECM remodeling, and neovascularization of microvessels and vasa vasorum without relying on systemic immunosuppression or *ex vivo* cell seeding. Despite significant progress, and particularly the remarkable completion of Symvess™ clinical trials, the first ever FDA approved TEVG, safety and efficacy in a pediatric population have not been established, and no off-the-shelf TEVG has yet demonstrated consistent long-term (>36 months) patency in clinical settings superior to autologous grafts. When Symvess™ was applied to treat extremity vascular injuries on 54 patients' primary patency was 58.3% with complications that included surgical site/device infections (20%), thrombosis (14%), vascular stenosis (6%), death (11%) and graft rupture at 1 year (4%) [23]. Key TEVG limitations that persist include poor endothelialization, inappropriate mechanical compliance, and inadequate structural biomimicry of native vessel layers [19, 24, 25].

Native veins and arteries are characterized by a hierarchical architecture including three histologically distinct layers, tunica intima, media, and adventitia, based on cellular and tissue constituents that are specialized to fulfil highly specific organ functions.

Based on these considerations, we hypothesize that a biomimetic, multilayered architecture that recapitulates structural heterogeneity of a native vessel may improve functional integration and long-term performance of TEVGs. To test this notion, in this work, we present a three-layered vascular graft (3LVG) that integrates structural and biochemical cues to guide host cell infiltration and its consequential tissue remodeling. The 3LVG combines (i) an electrospun (ES) fiber-dense polyurethane layer, (ii) a central bioactive layer of porcine small intestine submucosa-derived ECM, and (iii) a porous layer fabricated by thermally induced phase separation (TIPS).
The overall premise of this study is that establishing a structural gradient, based on differential scaffold porosity and bioactivity across the graft wall, will direct host cell infiltration in a manner that reduces intimal hyperplasia and enhances vascular remodeling. To challenge this hypothesis, two 3LVG configurations were fabricated: one promoting a cell infiltration route from the intimal side (Intima Cell Recruitment (ICR): TIPS-ECM-ES), and the other favoring adventitial infiltration (Adventitia Cell Recruitment (ACR): ES-ECM-TIPS).
By integrating biomaterials engineering with *in vivo* validation, this work supports biomimicry as an effective design paradigm to develop the next generation of small-diameter TEVG, addressing a critical bottleneck in achieving better outcomes in cardiovascular surgery.

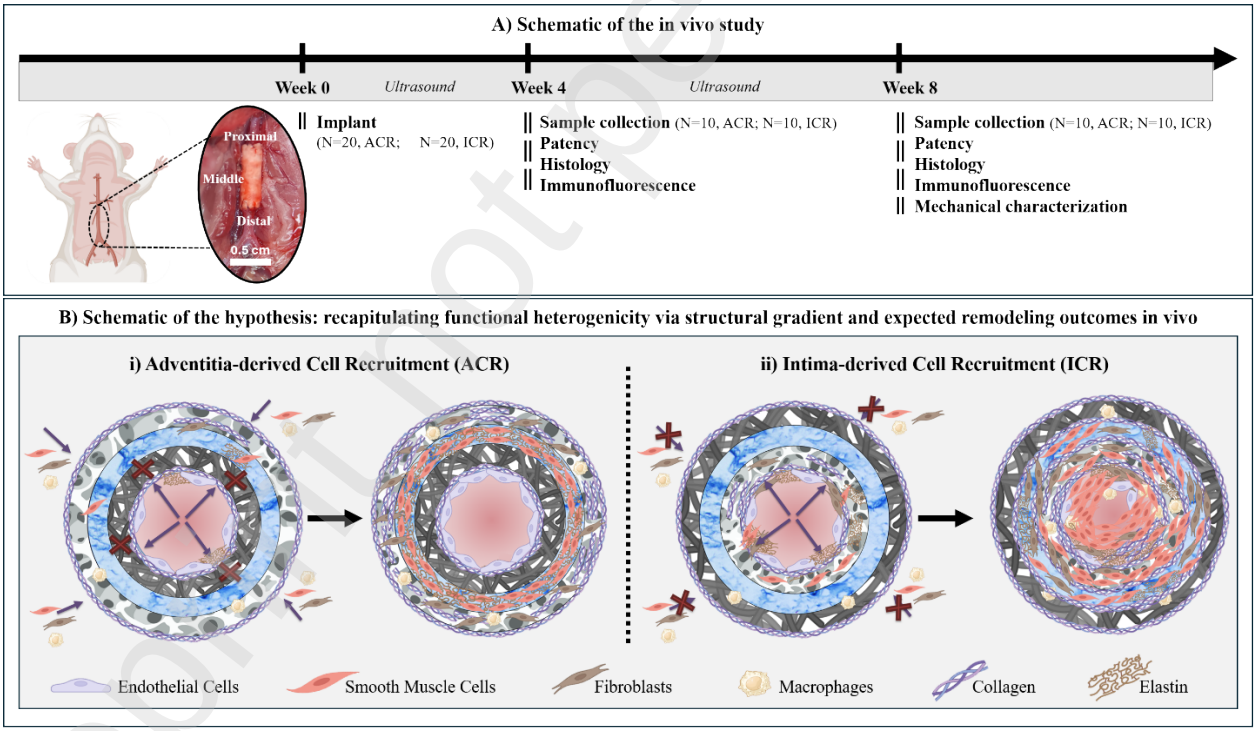

Figure 1: Overview of the in vivo assessment and hypothesis of the study. *A) Schematic of the in vivo study. Two 3LVG configurations, ACR and ICR, were implanted as abdominal aorta interposition graft in a rat model (Sprague Dawley, N=40). In vivo performance, patency, biomechanics and remodeling were assessed at 4 weeks and 8 weeks. B) Schematic of the hypothesis: recapitulating functional heterogeneity via structural gradient and expected remodeling outcomes in vivo: i) in the ACR configuration, the porous TIPS adventitia layer is expected to facilitate cell infiltration from the surrounding tissue, while the fiber-dense ES intima layer supports luminal cell attachment and limits transmural cell migration. These biomimetic structural gradients, mimicking native tissue functional*

heterogeneity, will promote cell infiltration, migration, and the deposition of de novo tissue, leading to the formation of a vessel-like construct with histologically distinct tunicae; ii) in contrast, in the ICR configuration is expected to restrict cell infiltration within the ES adventitia layer, while promoting cell infiltration and proliferation within the TIPS intima layer. This inverted architecture may induce cellular expansion at the luminal interface, finally contributing to intimal hyperplasia and progressive graft occlusion.

2. Materials and Methods

The 3LVGs were designed and developed to mimic the native tunicae functions of the coronary artery (intima, media, and adventitia). The tunica media was reproduced as a bioactive layer composed of decellularized ECM-based gel. While the adventitia and intima layers were manufactured by TIPS and ES techniques. Poly(carbonate-urethane)urea (PCUU), a synthetic polymer, was chosen to fabricate the TIPS and ES layers due to its biocompatible and biodegradable properties [26]. PCUU was synthesized following the previously reported procedure [27].

2.1. Design, development, and characterization of the 3LVG

2.1.1. Biofabrication of the three layers

Fibrous layers

Microfiber layers were generated using electrospinning (ES) to produce fiber-dense microarchitecture. PCUU was dissolved as 12% (w/v) in 1,1,1,3,3,3-hexafluoro-2-propanol (HFIP). 1.65 mm (mandrel for the intima layer) and 2.00 mm (mandrel for the adventitia layer) diameter stainless steel rods were adopted for electrospinning as targeting charged at -3 kV, rotating at 150 rpm, and translating longitudinally at 1.5 cm/s. The positive voltage of the PCUU polymer stream was at +3 kV, and its flow rate was 1.5 mL/h. After the electrospinning process, rods were cooled in liquid nitrogen to facilitate scaffold extraction. The electrospun grafts were then sterilized using ethylene oxide prior to the *in vivo* study.

Porous layers

Porous layers were fabricated using thermally induced phase separation (TIPS) to achieve a highly porous architecture. PCUU was dissolved in dimethyl sulfoxide (DMSO) as 8% (w/v) at 80°C. The solution was collected using a syringe with a 23-gauge needle and injected into pre-heated intima and adventitia custom-made molds, respectively. The molds were rapidly cooled at -80°C for 3 h for the formation of an interconnected porous structure. Then, the molds were immersed into an 70% ethanol solution at -20 °C, and the ethanol solution was exchanged with fresh 70% ethanol several times for DMSO extraction. After 15 days, the porous scaffolds were collected from the mold and washed in deionized water at 4°C to remove residual solvent, then freeze-dried for 42 h and sterilized using ethylene oxide.

Bioactive media layer: decellularized porcine small intestine submucosa (SIS) ECM-based gel

Porcine SIS without mesentery was purchased by Animal Biotech Industries (ABi, Inc.). The superficial layers of the tunica mucosa were mechanically removed from porcine jejunum and the tissue was treated following the protocol described in [28]. Likewise, the tunica serosa and tunica muscularis externa were mechanically removed, leaving the tunica submucosa and basilar portions of the tunica mucosa. Decellularization and disinfection of the tissue were completed by agitation in 0.1% (v/v) peracetic acid with 4% (v/v) ethanol for 2 h at 300 rpm. The tissue was then extensively rinsed with PBS and sterile water. The SIS was then lyophilized and milled into particulate using a Wiley Mill with a #40 mesh screen. To obtain a decellularized SIS ECM-based gel, the ECM decellularized powder was enzymatically digested at a concentration of 40 mg

ECM/mL and 20 mg/mL using 2 mg/mL pepsin in 0.01 M of HCl for 48 h at room temperature with constant stirring. For the gelation, digested ECMs were neutralized on ice adding a solution of 1:10 of the digested volume of 0.1M NaOH and 1:9 the digest volume of PBS 10X and further diluted to a final ECM concentration 16.5 mg/mL using PBS 1X.

Assembling of the 3LVGs

The polymeric intima layer (TIPS or ES) was positioned onto a cylindrical support (ID: 1 mm). Both extremities were secured to the support using a 7-0 polypropylene suture (M8303, Ethicon). Subsequently, the polymeric adventitia layer (ES or TIPS) was inserted into the polymeric intima layer (TIPS or ES) and sutured at the distal extremity. Following neutralization, ECM gel was injected between the two layers using a 23-gauge straight needle. This injection was conducted under a dissecting microscope (Nikon SM Z25) to ensure thorough filling of the space between the polymeric layers with the bioactive gel. The 3LVG was then placed in an oven at 37°C for 1 h to facilitate the gelation of the ECM-based layer. Afterward, the sutures were removed, and the 3LVG was trimmed to a length of 1 cm.

2.1.2. Characterization of the three layers and the assembled 3LVGs pre-implant

Morphological evaluation of the porous and fibrous adventitia/intima layers

Electrospun adventitia/intima and TIPS adventitia/intima layers were characterized using Scanning Electron Microscopy (SEM, JEM-6335F, JEOL) to investigate surface, fiber and pore morphology. Before the analysis, the samples were sputter-coated with 5 nm of gold-palladium (Sputter Coater 108 auto, Cressington Scientific Instruments). SEM images were analyzed using NIH-ImageJ software (Bethesda, Maryland, USA, https://imagej.nih.gov/ij) to evaluate the thickness, the pore dimension of each layer and the fiber mean diameter of the electrospun layer. For this purpose, five randomly chosen images were selected for each adventitia/intima layer.

Macroscopical evaluation of the assembled 3LVGs

The cross-section of the 3LVGs was macroscopically investigated by acquiring images through a dissecting microscope (Nikon SM Z25) to assess presence and continuity of the bioactive ECM layer between the two polymeric layers and to check the graft's wall thickness.

Suture retention test of the assembled 3LVGs and native rat abdominal aorta

The suture retention strength of the ACR, ICR 3LVGs, and native rat abdominal aorta was determined using an MTS Insight® Electromechanical Testing Systems with a load cell of 100 Newton following the *ISO 7198:2016: "Cardiovascular implants and extracorporeal systems – Vascular prostheses – Tubular vascular grafts and vascular patches"*. The 3LVGs (N=4 for each configuration) and native rat abdominal aorta (N=15) were clamped distally in the tensile testing setup. A monofilament 7-0 polypropylene (M8303, Ethicon) suture was used to create a single loop 2 mm away from the sample's edge (**Figure 2D**). The free ends of the suture were secured to the upper clamp. The samples were then pulled at a rate of 60 mm/min. The maximum force required to pull the suture through the sample was considered as the suture retention strength.

Global compliance test of the assembled 3LVGs and native rat abdominal aorta

The global compliance of the ACR (N=5), ICR (N=6) 3LVGs, and native rat abdominal aorta (N=6) was investigated using a custom-made device [29]. A 7-0 polypropylene (M8303, Ethicon) suture was used to secure the graft and the native tissue to a precision guide needle. Hydrostatic pressure (steps of 0, 50, 80 and 120 mmHg) was generated using a 10 L tank filled with water and placed at different heights (**Figure 3B**). A programmable PHD 2000 Harvard Apparatus syringe pump with a 60 mL syringe was used to generate a constant flow (10 mL/min) in the circuit. The samples were fully submerged in water at room temperature. Ten images of the entire vessel were captured at each pressure value using a Canon EF 50 mm f/2.5 Compact Macro Lens. The pressure

signal was acquired with a SPR-320 Mikro-Tip pressure catheter (Millar) equipped with a PCU-2000 pressure control unit (Millar) and recorded with LabVIEW. Data postprocessing was performed by a custom-made script developed in MATLAB where vessel diameters were calculated by digital image analysis and correlated to the corresponding pressure value. Global compliance (C) was calculated following this formula [30, 31]:

$$C = \frac{(OD\ 120 - OD\ 80)}{\frac{OD\ 80}{(P\ 120 - P\ 80)}}$$

with *OD* being the vessel outer diameter and *P* the pressure at 80 mmHg and 120 mmHg.

2.2. *In vivo* study

All the procedures and experiments were approved by and performed according to the guidelines of the Institutional Animal Care and Use Committee (IACUC) at the University of Pittsburgh under the protocol IS00024256 "*Three-layered, bio-inspired, small-diameter vascular graft for tissue engineering applications (3)".* Animals were euthanized in accordance with the guidelines of the American Veterinary Medical Association (AVMA) Panel of Euthanasia. **Error! Reference source not found.** shows a schematic of the *in vivo* study and explants characterization.

2.2.1. Rat aorta replacement surgery

Both configurations, ACR and ICR 3LVGs, were implanted into the abdominal aorta of female Sprague Dawley rats (Envigo, 200-300g) with N=10 for each group (ACR and ICR) and time point (4 and 8 weeks). First, the animal was anesthetized with isoflurane (2 % for induction and 1 % for maintenance). The rat was placed in a supine position on a warming blanket (37 ℃) and the abdomen was shaved and prepared with povidone-iodine solution. Due to a midline laparotomy incision, the abdominal aorta was exposed below the renal arteries. Before the aortic clamp was applied, sodium heparin (100 IU/Kg) was administered. Microclamps were used to fix the infra-renal aorta, proximally and distally and the rat aorta was sectioned between the clamps creating a gap of 0.5-0.7 cm. Then, the 3LVG was sutured in place to replace the native abdominal aorta in an end-to-end interrupted anastomosis with 10-0 nylon suture. After the 3LVG was anastomosed, the microclamps were removed and the patency and leakage of the 3LVG were assessed by direct observation. Finally, the muscle layer and skin were closed with 4-0 polyglactin absorbable suture and the rat was observed in the surgical suite until fully recovered from anesthesia and then returned to the housing area. All the surgical procedures were conducted utilizing a surgical stereo microscope (Carl Zeiss). Each rat received 0.1 mg/Kg buprenorphine intramuscularly one time after operation and twice per day for 3 days after surgery for analgesia. Cefazolin (100 mg/Kg) was injected intramuscularly once before the operation and twice for 2 days postoperatively to prevent surgical site infection. Aspirin (5 mg/Kg) and dipyridamole (200 mg/kg) were administrated daily for the entire duration of the study until sacrifice.

2.2.2. Function and performance of the 3LVG *in vivo*

In vivo ultrasound analysis

Ultrasound analysis was used to evaluate graft patency and was performed using the Acuson Sequoia C256 system with a 13 MHz linear ultrasonic transducer (15L8, Acuson Corporation, Mountain View, California). All the data was collected for each animal before the surgery and at 2, 4, and 8 weeks post-implantation. To perform the analysis, the rat was anesthetized with isoflurane (3% for induction and 1% for maintenance), placed into a supine position on the warming pad (37°C) and abdominal hair was removed. The 3LVG was imaged longitudinally and

the average maximum velocity inside the implant was recorded using a pulse Doppler mode. Patency was defined as an observable blood flow under color doppler imaging.

Computed tomography scan analysis

Computed tomography (CT) scan analysis was performed to assess the patency of the graft just before animal sacrifice [32]. Systemic heparinization (0.8cc of sodium heparin) under heartbeat into the inferior vena cava). The rat was euthanized and an 18-gauge angio-catheter was placed in the thoracic descending aorta and secured with a 2-0 silk suture to inject ISOVUE-300 (Bracco Diagnostics) as a contrast agent. The patency rate was calculated as the number of animals with positive contrast flow through the 3LVG over a total surviving number of animals within each group and time point.

2.2.3. Characterization of the 3LVGs explants

After the CT analysis, the 3LVG was explanted from the animal and washed three times gently. Gross macroscopic analysis was performed using a dissecting microscope (Nikon SM Z25) to investigate the presence of intraluminal thrombus. Then, the explanted 3LVGs at 4 and 8 weeks were further characterized at macro and microscopic level.

Macroscopic analysis

The 3LVG explants were fixed in 10 % (v/v) of neutral buffered formalin for 24 h at 4°C and then washed three times in PBS 1X. Under a dissecting microscope, the 3LVGs were divided into 3 equal portions: proximal, middle, and distal. Cross-sectional images of the three portions were acquired (3X magnification) to investigate the macroscopic morphology and the presence of thrombus and neointima formation.

Histological evaluation

OCT-embedded 3LVGs and rat abdominal aorta were cryo-sectioned and stained with Hematoxylin and Eosin (H&E), Masson's Trichrome (MT), and Verhoeff-van Gieson (VVG) to evaluate cellular content and structural constituents of newly formed tissue such as collagen, elastin deposition, cellular infiltration, presence of neointima and vasa vasorum. Images of the whole cross-sections were acquired using an automatic brightfield microscope (MoticEasy Scan Pro 6 Digital Slide Scanner, Motic®) at 40X magnification. The histological inspection of the explants at 4 and 8 weeks was coupled with semi-quantitative measurements. Custom-made algorithms developed in MATLAB were utilized to segment and quantify the thickness of the neointima, the percentage of the patency area, the deposition of nascent collagen deposition and the number of infiltrated cells.

More specifically, a dedicated 'Neo-Intima Thickness Percentage Script' processes output images. From the centroid of the isolated neointima ring the scripts generate 100 segments, each time a segment encounters the denoted ring it starts counting the pixel till it finds black again and validates thickness measurements against manual ImageJ measurements.

The 'Patentcy Area Percentage and Neointima Percentage Script' generates binary masks for segmenting specific regions, using functions to threshold RGB values and refine masks to calculate lumen area and neointima area.

A 'Collagen Remodeling Script' analyzed MT images by segmenting the scaffold layers and collagen, also through the RGB thresholding process, binarizing, filtering masks, summing white pixels and converting them to an area measurement.

Finally, a 'Cell Recruitment and Counting Script' processed H&E images by segmenting through the thresholding process for cells, scaffold materials, and ECM using RGB masks. This allows users to manually refine regions using Matlab roipoly, isolating adventitia and intima layer scaffold materials and removing fibrotic tissue and neointima, with mask refinements done through

matrix operations. The Matlab regionprops function then extracted cell properties like centroid and equivalent diameter and tallies cells in each region.

Immunofluorescence evaluation

For the immunofluorescence analysis, frozen cross section of the samples was brought at room temperature for 30 min and rehydrated in PBS for 10 min. Antigen retrieval was achieved using Trypsin/EDTA solution (Sigma) at 37°C for 10 min. Next, the sections were washed in PBS and incubated with 2% (w/v) of BSA (Sigma), 10% (v/v) Goat Serum (Gibco) and 0.2% (v/v) Triton (Sigma)/PBS for 1 h. Following blocking, all samples were incubated with a primary antibody at room temperature. α-smooth muscle actin (αSMA, 1:200, ab7817, Abcam), and Von Willebrand factor (VWF, 1:200, ab6964, Abcam) were used to detect smooth muscle cells and endothelial cells, respectively. After primary antibody incubation and washing, the samples were further incubated for 1 h at room temperature with Alexa fluor 488 Goat Anti-Rabbit (1:200, A11008, Thermo Fisher) and Alexa Fluor 555 Goat Anti Mouse (1:200, A21424, Thermo Fisher), respectively. Each sample was then washed and counterstained with DAPI mounting medium (H-2000, Vectrashield® Plus Antifade Mounting Medium with DAPI).

Immunolabeling of each marker was imaged using the Axio Observer (Z1 Fluorescence, Carl Zeiss) at 20X magnification. The channel exposure time was consistent between each sample so that semi-quantitative analysis could be performed. The signal analysis was performed using a custom-made Matlab script for the semi-quantification of each marker.

Global compliance

ACR (N=4) and ICR (N=3) explants at 8 weeks were snap-frozen in 2-Methylbutane (Isopentane, Fischer Scientific) and cooled on dry ice for 3 minutes. Frozen samples were stored at -80°C. Before the analysis, the frozen explanted 3LVGs were thawed at 4°C overnight and rinsed in PBS 1X for 1 h before testing. The data analysis was carried out using the procedure previously described [33].

Vasa Vasorum

Adventitial vasa vasorum were quantified using H&E staining. For explanted specimen, three random images were analyzed by 5 independent human operators to determine the total number of vasa vasorum.

2.3. Statistical analysis

Statistical analysis was performed using GraphPad Prism 10.0 (GraphPad Software, Boston, Massachusetts, USA, www.graphpad.com). One-way or Two-way analysis of variance (ANOVA) followed by Tukey's multiple comparison test was used for comparison among multiple samples. Results are presented as average ± standard deviation or average ± standard error with differences considered to be statistically relevant when $p<0.05$ using post hoc analysis.

3. Results

Morphological characterization and suture retention test

Two configurations of the 3LVGs, ACR and ICR (**Figure 2A**), were fabricated and characterized to investigate the effects of functional heterogeneity on *in vivo* remodeling. Functional heterogeneity was implemented via the structural gradient created by the three distinct layers and the different pore sizes of the TIPS and ES layers. As shown in **Figure 2B**, the three layers of assembled ACR and ICR grafts were shown macroscopically to be integrated, and the ECM-gel based media layer was uniformly distributed throughout the entire two tubular structures (ES/TIPS layers). The 3LVGs designed for the *in vivo* study were 1 cm long and with an inner diameter of

1.4 ± 0.1 mm for the ACR configuration and 1.4 ± 0.1 mm for the ICR configuration, respectively measured using SEM. The inner diameter of the 3LVGs was uniform across configurations.
SEM revealed the average thickness of each layer of the ACR graft configuration was 63 ± 13 μm for the ES intima layer and 272 ± 40 μm for the TIPS adventitia layer, respectively (**Figure 2C**). For the ICR configuration, the average thickness was 124 ± 32 μm for the TIPS intima layer and 96 ± 7 μm for the ES adventitia layer, respectively. The polymeric TIPS intima layer in the ICR graft was thicker compared to the polymeric ES intima layer in the ACR graft. This was attributed to the limitations of the TIPS fabrication technique in achieving a homogenous tubular structure with less than 100 μm using a thinner mold. SEM characterization confirmed porous morphology for the TIPS layers and fiber morphology for the ES layers. In detail, cross section, inner and outer surfaces of the ES layers exhibited a homogeneous nonaligned randomly fibrous network. The average fibers diameter was measured as 0.8 ± 0.2 μm and 0.9 ± 0.3 μm for the intima and adventitia ES layers, respectively. The TIPS layers were characterized by random-shaped and interconnected pores. Overall, the pore size responsible for the scaffold structural gradient ranged 6-23 μm (ES) and, 30-100 μm (TIPS). Rat abdominal aortas were characterized by histological analysis to extract information regarding the inner diameter, the thickness of the intima and media layers, the thickness of the adventitia layer, and wall thickness. These data were compared to the thickness of the intima and media layers for each configuration (**Table 1****Table 1:** Experimental measurement of the inner diameter, and layer thickness for each 3LVGs configuration and rat abdominal aorta (*). Measurement obtained by SEM imaging (**). Measurement obtained by MT histological imaging analysis. For each group, N=4 independent samples were analyzed.).

Table 1: Experimental measurement of the inner diameter, and layer thickness for each 3LVGs configuration and rat abdominal aorta (*). Measurement obtained by SEM imaging (**). Measurement obtained by MT histological imaging analysis. For each group, N=4 independent samples were analyzed.

	Adventitia-derived Cell Recruitment (ACR)	**Intima-derived Cell Recruitment (ICR)**	**Rat Abdominal Aorta (Rat Abd Aorta)**
Inner Diameter	1.4 ± 0.1 mm*	1.4 ± 0.1 mm*	1.4 ± 0.1 mm*
Intima Thickness	63 ± 13 μm* ES layer	124 ± 32 μm* TIPS layer	72 ± 11 μm** Intima+Media layers
Adventitia Thickness	272 ± 40 μm* TIPS layer	96 ± 7 μm* ES layer	143 ± 59 μm**

The suture retention strength for ACR and ICR pre-implant 3LVGs was measured as 1.9 ± 0.1 N and 1.8 ± 0.1 N, respectively. Both configuration ACR and ICR 3LVGs had a similar suture retention force (**Figure 2**, **D**), which was higher ($p<0.001$) than that of the native rat abdominal aorta of 1.2 ± 0.3 N.

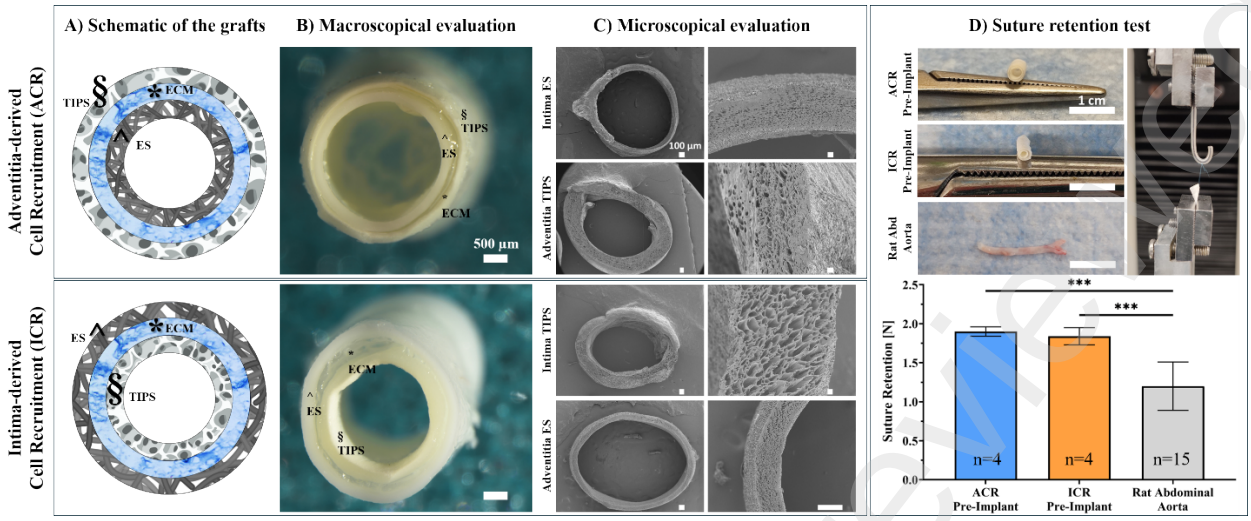

Figure 2: Overview of the 3LVG ACR and ICR configurations. A) Schematic of the grafts with layers labelled as follows: ^: ES layer, *: ECM layer and §: TIPS layer. B) Macroscopical and C) microscopical evaluation of the ACR and ICR 3LVG configurations. SEM images of the full cross section and higher magnification views of the polymeric intima and adventitia layers highlighting an order of magnitude difference in pore size between the TIPS and ES layers. D) Suture retention test. All data were reported as the mean ± STD. One-Way ANOVA was utilized for statistical analysis with * $p<0.05$. Sample size (n) is indicated in each bar.

In vivo functional performance and global compliance

Animals were implanted with ICR or ACR 3LVGs. After graft implantation, all the rats were examined for bleeding (Supplementary Video S1). There were few (3 animals) mortalities due to preprocedural complications such as anesthesia; no bleeding was found on the anastomotic sites of the implanted graft in the other animals. Animals were euthanized after 4 and 8 weeks for both ICR and ACR groups, for a total of four experimental groups: 1) ICR 4 weeks; 2) ICR 8 weeks; 3) ACR 4 weeks and 4) ACR 8 weeks. Doppler ultrasound was successfully completed in 22 animals at the designated time points (**Figure 3A**). Patency was evaluated by visual observation, histology, CT angiography and echography. Overall, 34 out of 37 grafts were patent (91.9%). Specifically, 50% of the ICR grafts remained patent at 4 weeks and 75% at 8 weeks. In contrast, ACR grafts showed superior patency, with 83% patent at 4 weeks and 100% at 8 weeks. Downstream flow abnormalities, including spectral broadening and turbulence, were observed and interpreted as post-stenotic changes. Importantly, no intraluminal thrombus or aneurysmal dilatation was detected. Doppler ultrasound revealed focal luminal narrowing, likely due to anastomotic mismatch.

The global compliance of the ACR and ICR 3LVGs was assessed both pre-implantation and at 8 weeks post-implantation (**Figure 3B**)**Error! Reference source not found.** Compliance measurements were conducted at 80 mmHg and 120 mmHg to simulate physiological conditions. As shown in **Figure 3B**, the global compliance values were $7.5 \pm 0.8 \times 10^{-4}$ mmHg and $1.7 \pm 0.9 \times 10^{-4}$ mmHg for the ACR (N=5) and ICR (N=6) grafts, respectively, prior to implantation, and $9.5 \pm 0.9 \times 10^{-4}$ mmHg and $6.0 \pm 1.6 \times 10^{-4}$ mmHg for ACR (N=4) and ICR (N=3) grafts at 8 weeks post-implantation. The 3LVGs results were compared to the native rat abdominal aorta (N=6), which showed a compliance value of $10.9 \pm 0.4 \times 10^{-4}$ mmHg. There was no significant difference in the compliance of the ACR grafts at 8 weeks post-implantation compared to the native rat abdominal aorta.

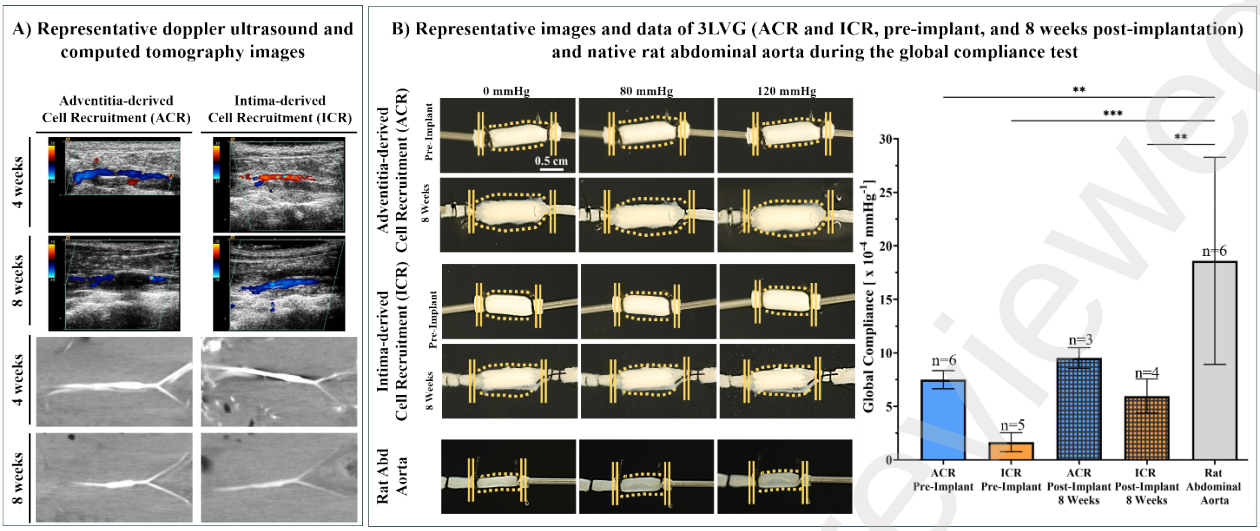

Figure 3: In vivo performance and global mechanical compliance of the 3LVGs. *A) Representative doppler ultrasound and computed tomography images of ACR and ICR grafts at 4 and 8 weeks post-implantations. B) Representative images of 3LVGs (ACR and ICR, pre-implant and 8 weeks post-implantation) and native rat abdominal aorta during the global compliance test at 0, 80, and 120 mmHg. Global compliance of the 3LVGs pre-implant (N=5 for ACR and N=6 for ICR, respectively) and post-implant at 8 weeks (N=4 for ACR and N=3 for ICR, respectively). The data were compared to the native rat abdominal aorta (N=6). Data are presented as mean ± STD. One-Way ANOVA was utilized for statistical analysis with * $p<0.05$.*

Gross examination of the explants and thickness of the neointima

Both ACR and ICR 3LVGs were simple to handle and demonstrated adequate suture retention force. Additionally, there was no observed bleeding through the anastomosis or along the entire length of the grafts.

During the surgical procedure, prior to implantation, two animals in the ICR group (one in the 4-week group and one in the 8-week group) and two animals in the ACR group (one in the 4-week group and one in the 8-week group) died for unknown causes. For the measurements of the patency rate at 4 weeks for the ICR group, one animal was not considered due to the observation by histological analysis of surgical failure. However, all the remaining animals survived to their respective endpoints.

Gross examination of the explants revealed that both configurations were well integrated with the surrounding native tissue (**Figure 4A**). The inner surfaces of all patent grafts displayed no evidence of clot formation and were covered by a collagenous layer. The presence of neo-vasculature around the 3LVGs was observed in both configurations at 4 and 8 weeks. None of the patent grafts showed signs of acute inflammatory response or infection. Macroscopic observation and histological analysis indicated that the two occluding cases within the ICR group, observed at 4 and 8 weeks, were attributable to intimal hyperplasia.

The patency rate, observed macroscopically, was 100% (9/9) for the ACR group at 4 and 8 weeks (9/9), 100% (8/8), and 80% (8/10) for ICR at 4 weeks and 8 weeks, respectively (**Figure 4B**).

Quantitative histological analysis revealed that the thickness of the neointima (**Figure 4C**) exceeded 100 µm in both configurations, ACR and ICR, at 4 and 8 weeks. In detail, the measurements for the ACR group at 4 weeks (N=8) and 8 weeks (N=5) were as follows: proximal segment 145 ± 38 µm VS 190 ± 4 µm, middle part 103 ± 54 µm VS 132 ± 33 µm and distal part 85 ± 19 µm VS 121 ± 32 µm. Additionally, for the ICR configuration at 4 weeks (N=6) and 8 weeks (N=4), the thickness values of the neointima were: proximal part 172 ± 138 µm VS 131 ± 44 µm, middle part 132 ± 127 µm VS 110 ± 41 µm and distal part 73 ± 31 µm VS 117 ± 31 µm.

In order to perform a comprehensive assessment of the 3LVG *in vivo*, measurements of the neointima thickness also included samples in the proximal region where values were more pronounced when compared to the medial or distal segments. This explains the high variability in the ICR groups at 4 weeks where some samples exhibited stenosis in the proximal segment. Despite the thickness > 100 µm, the % of neointima in comparison to the % patency area of the 3LVGs (ACR and ICR) was 17 ± 6 % for ACR (N=8) and 18 ± 10 % for ICR (N=6) at 4 weeks and 21 ± 7 % for ACR (N=5) and 20 ± 6 % for ICR (N=4) at 8 weeks. Consequently, the free area (% patency area) available for blood flow, which is essential for maintaining an adequate supply, was 82 ± 7 % for ACR (N=8) and 82 ± 10 % for ICR (N=6) at 4 weeks and 78.98 ± 6.98 % for ACR (N=5) and 78.81 ± 6.13 % for ICR (N=4) at 8 weeks.

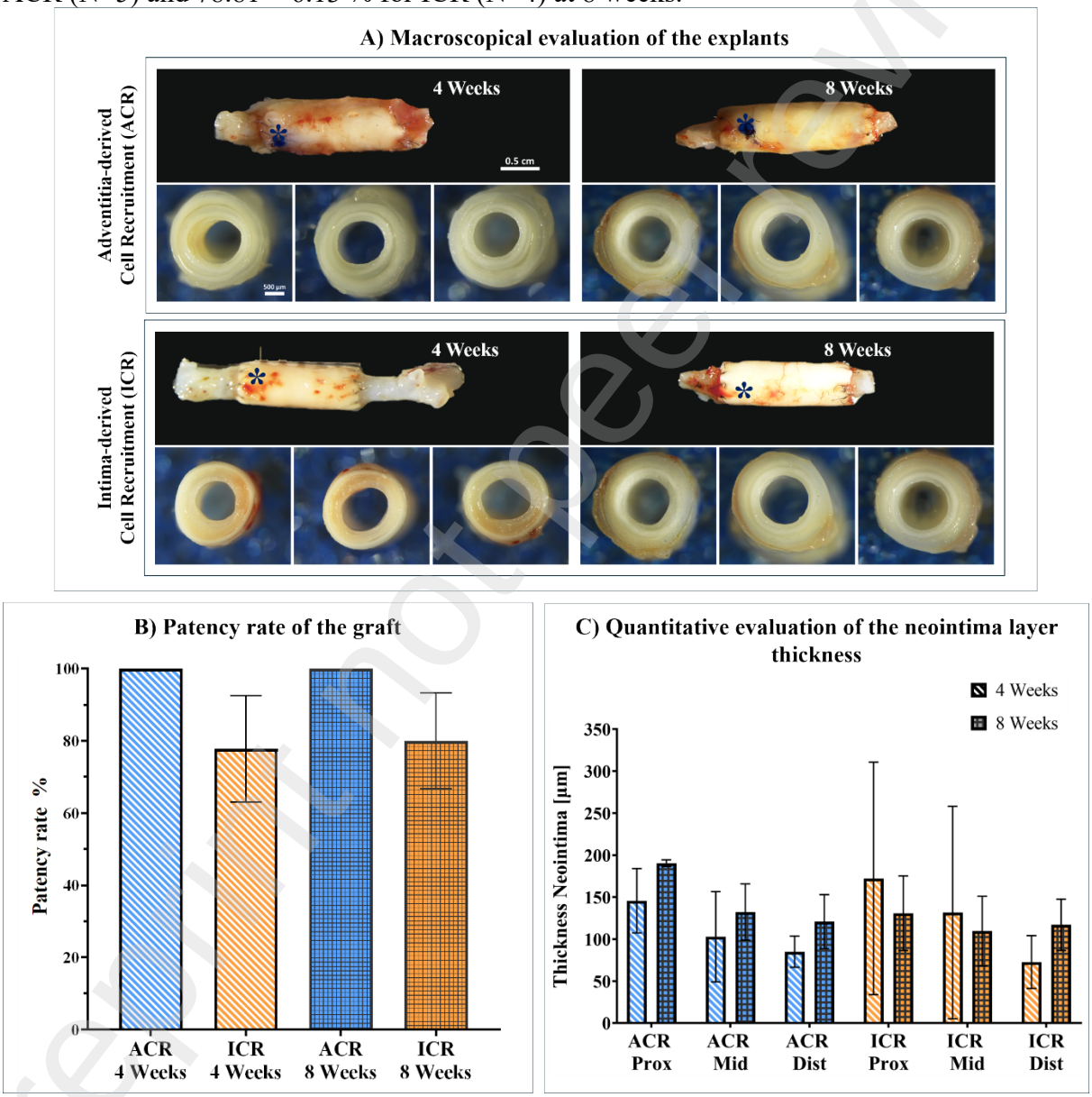

Figure 4: A) Macroscopical evaluation of the explant and patency rate after 4 weeks and 8 weeks of implantation. *A) Macroscopic observation of the explants. The blue asterisk in the image marks the proximal side of the explant. The cross-section represents the macroscopic view of the proximal, middle, and distal portions of the 3LVG for each configuration and time point. B) Patency rate of the grafts. C) Quantitative evaluation of the neointima layer thickness.*

*Data reported as mean ± STD. Two-Way ANOVA was utilized for statistical analysis with * $p<0.05$. For each 3LVG configuration and layer $N \geq 12$ images were analyzed.*

Histological characterization and quantitative analysis

Cell infiltration, de novo collagen, elastin deposition, and de novo ECM deposition were assessed using histological staining techniques. **Figure 5A** shows representative histological images of the middle segments from ACR and ICR 3LVGs explant at 4 weeks and 8 weeks, alongside the native rat abdominal aorta. Neointima formation was observed in both graft configurations. H&E and MT stains revealed that the neointima was rich in newly deposited ECM, in particular collagen, with comparatively lower levels of neo-elastin observed from VVG staining. The ECM-based gel media layer was still present in all the configurations. At 8 weeks, ACR configuration exhibited features consistent with surrogate vessel-like remodeling, characterized by neo-collagen deposition and notable cell infiltration within the adventitia TIPS layer (**Figure 5: Histological** **Figure 5B**).

MT stain highlighted collagen deposition surrounding both polymeric layers (ES and TIPS) in all explants. Specifically, the ACR configuration showed a higher collagen fraction compared to the ICR at both 4 and 8 weeks. The difference reached statistical significance at 8 weeks for the ACR intima layer, where collagen content was 44 ± 12% in comparison to the adventitia of the ICR at both time points and to the intima ICR at 8 weeks.

A quantitative cell infiltration analysis, conducted via H&E,(**Figure 5B**) across layers (adventitia, media and intima) at each timepoint showed, a slightly increased cell number at 8 weeks compared to the 4 weeks in the layers of the ACR configuration with a highest cell density observed in the adventitia layer (4 and 8 weeks: 2418 ± 1467 and 2965 ± 4094). Conversely, the ICR configuration exhibited a reduction in number of cells at 8 weeks compared to the 4 weeks across all layers.

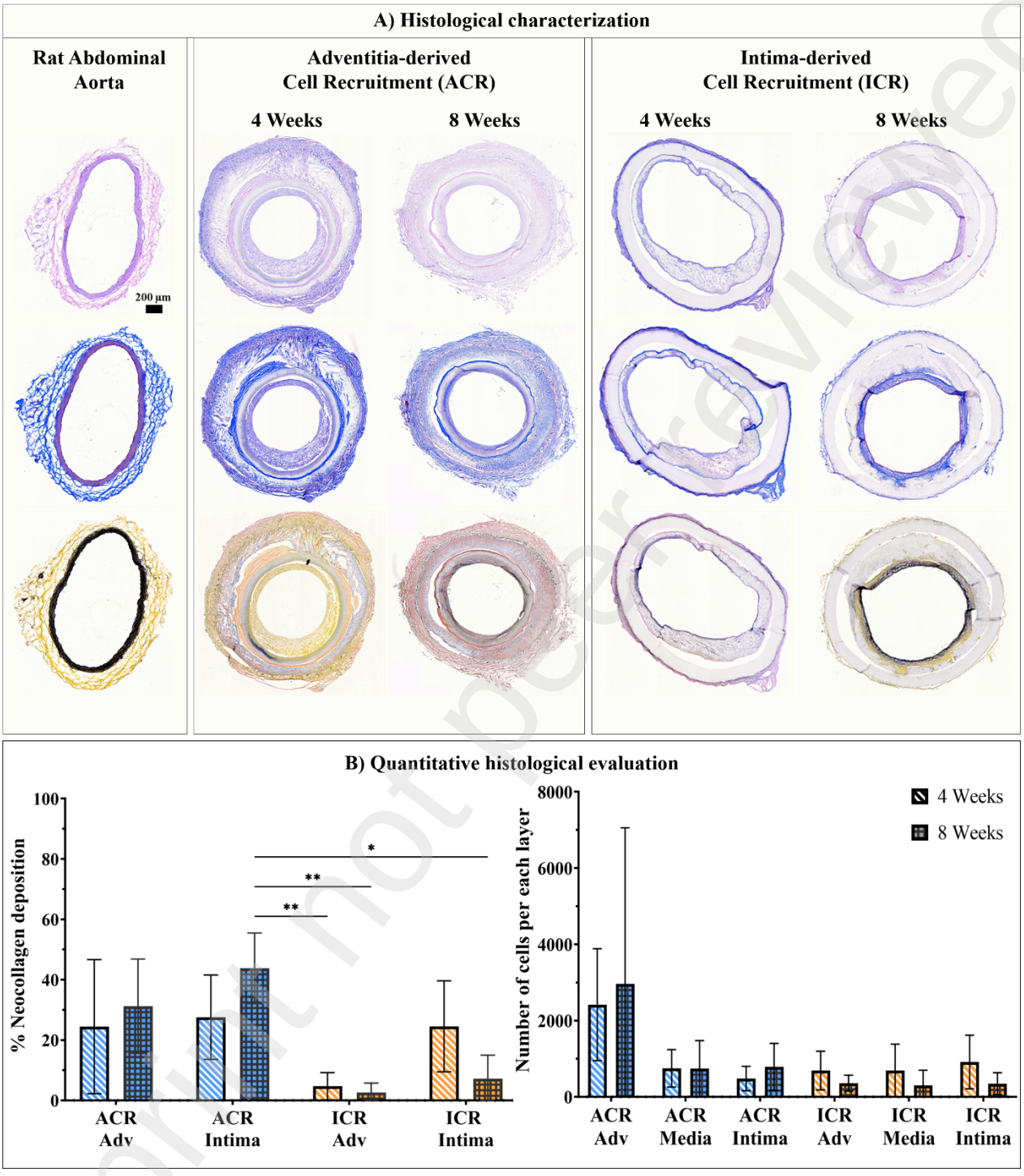

Figure 5: Histological assessment of ACR AND ICR 3LVG. *A) Histological characterization of the middle portion of the ACR and ICR 3LVGs explanted at 4 and 8 weeks in comparison to the native rat abdominal aorta. H&E, MT, VVG were used as staining. Scale bar: 200 µm. B) Quantitative histological evaluation. The % of neocollagen was quantified to investigate the remodeling of the 3LVGs. Collagen quantity and cell infiltration in the adventitia and intima polymeric layers were calculated with custom-made digital image analysis methods. Data reported as the mean ± STD. Two-Way ANOVA was utilized for statistical analysis with * $p<0.05$. For each 3LVG configuration and layer, $N \geq 12$ images were analyzed.*

Immunofluorescence characterization and quantitative analysis

Representative immunofluorescent images of the inner intimal location for both ACR and ICR explants at 4 and 8 weeks reveal detection of α-SMA, VWF, and cell nuclei (**Figure 6A)**. The signal intensity of these markers was semi-quantitatively assessed using image processing in Matlab. The results are shown in **Figure 6B.**

In the whole ACR and ICR grafts (neointima, intima, media, and adventitia layers), the total α-SMA signal was found to be equivalent across all groups at each time points. Luminal endothelialization of the constructs was evaluated using VWF marker. **Figure 6B** shows that the ACR groups at 4 and 8 weeks of implantation showed higher VWF signal compared to the ICR groups.

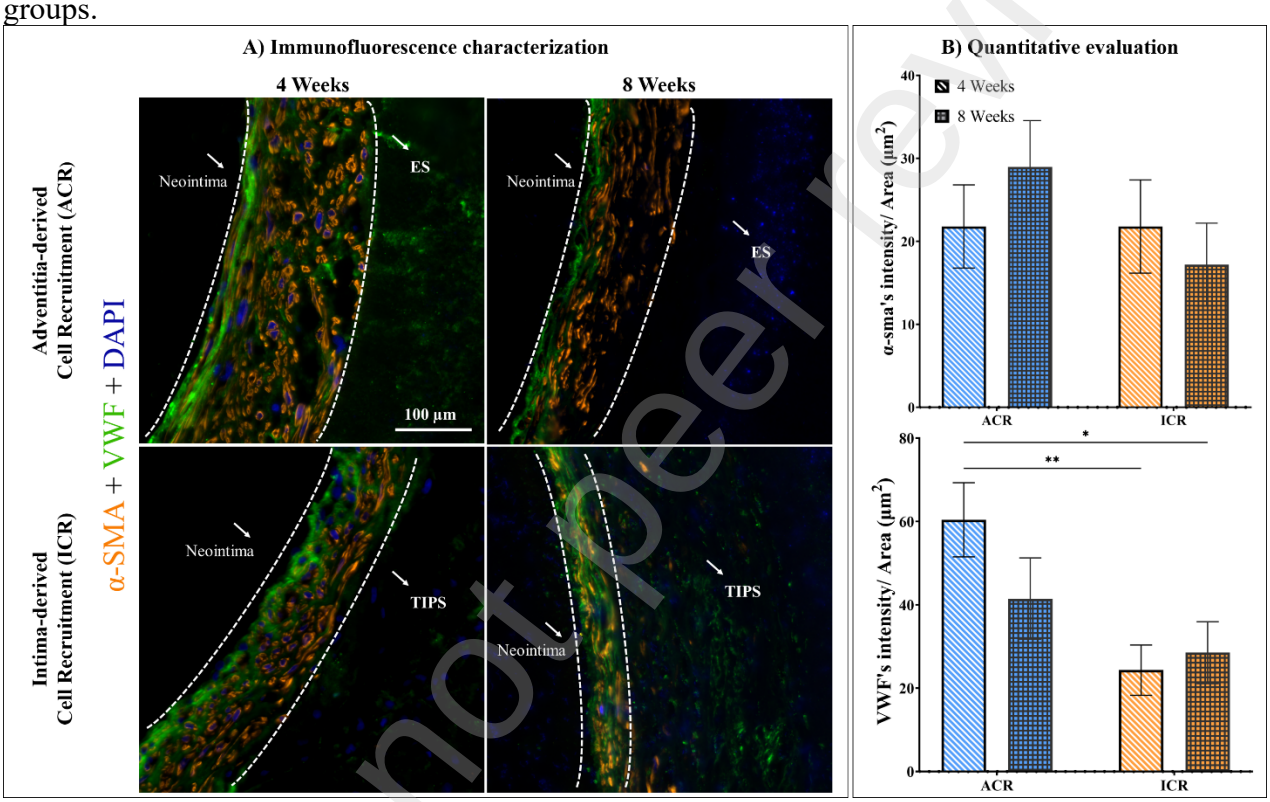

Figure 6: Immunofluorescence characterization of ACR and ICR 3LVGs. *A) Representative middle cross-sectional immunofluorescence images of the inner part of the TEVG configurations. Orange, green and blue represent the α-SMA marker, VWF marker and cell nuclei, respectively. The scale bar is 100 µm. B) Quantitative evaluation of the α-SMA and VWF content considering the whole device signal (neointima, intimal layer, medial layer and adventitial layer). For each 3LVG configuration, N ≥ 30 images were analyzed. Data reported as the mean ± ERR ST. Two-Way ANOVA was utilized for statistical analysis with * p<0.05.*

Vasa vasorum quantification

Representative images from ACR and ICR explants at 4 and 8 weeks demonstrate the presence of vasa vasorum within the de novo adventitia layer of all the 3LVGs (

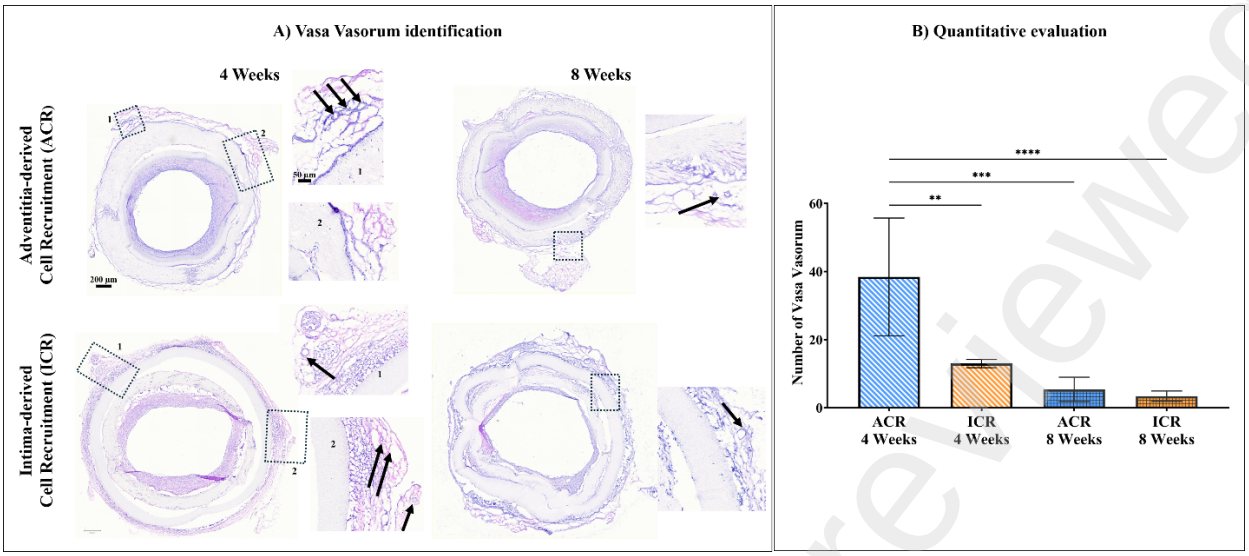

Figure *7*). Quantitative analysis highlighted significantly higher number of vasa vasorum in the ACR group at 4 weeks when compared with all other groups and time points (

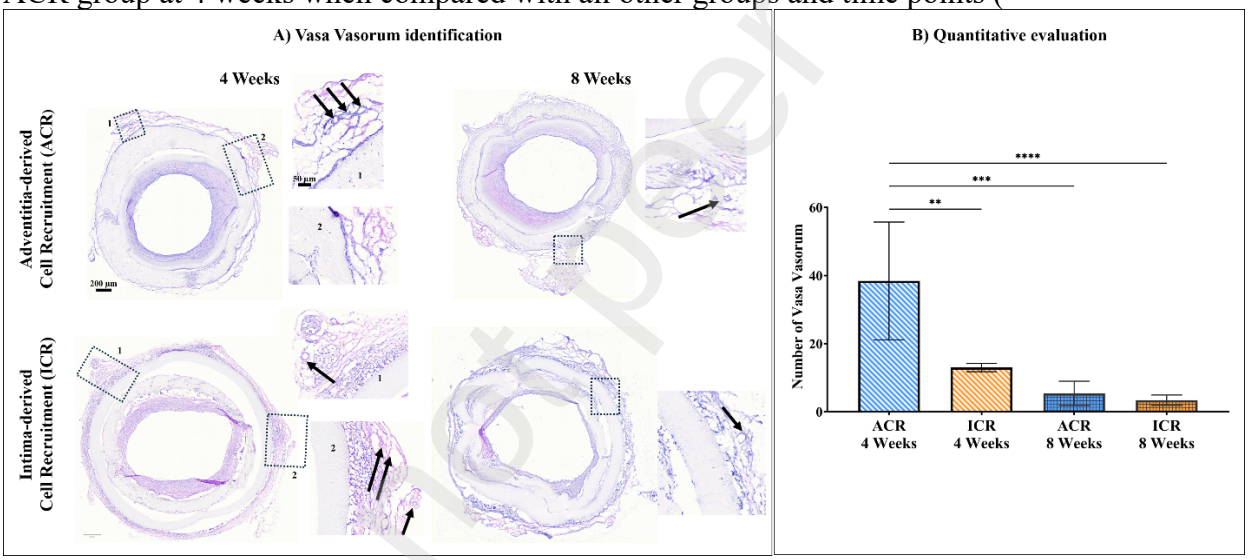

Figure *7***B**). Specifically, the ACR group at 4 weeks exhibited a number of 38 ± 17 vasa vasorum, in contrast to the ICR group at 4 weeks were only 13 ± 1 vasa vasorum were detected. At 8 weeks the number of vessels sensibly decreased with 5 ± 4 in the ACR group, and 3 ± 2 in the ICR group.

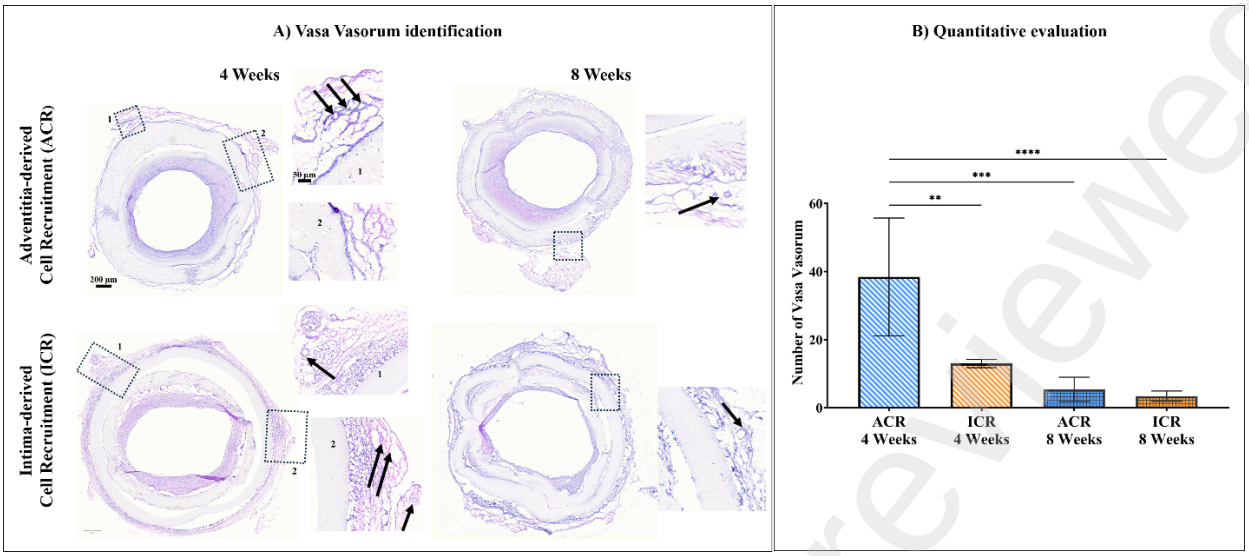

Figure 7: Vasa vasorum detection within the adventitia layer of ACR and ICR 3LVGs. *A) Representative cross-sectional histological images of ACR and ICR explants with the highlighted vasa vasorum detected in the neoadventitial layer. Scale bars are 200 µm for the cross-section and 50 µm for the inset images. B) Quantitative evaluation of the number of adventitial vasa vasorum. Data reported as mean ± STD. For each explant, N=3 distinct images were analyzed to detect vasa vasorum and neovascularized micro vessels.*

4. Discussion

In this study, we demonstrate that spatially controlled scaffold architecture, achieved through a structural gradient across the graft wall, plays a critical role in directing host-driven vascular remodeling. By integrating, electrospinning and TIPS, we engineered a three-layered vascular graft (3LVG) designed to recapitulate the functional heterogeneity of native vessels by modulating the distribution of infiltrating host cells. This multilayer strategy enabled independent control over fiber morphology, pore structure, and biochemical composition, thereby addressing key limitations of single-layer polymeric grafts. ES produced thin fibrous intimal and adventitial layers with reproducible microstructure and suture-handling properties, while TIPS generated an interconnected porous layer conducive to transmural cell migration and early remodeling. Dimensional tuning allowed the constructs to closely match the rat abdominal aorta, facilitating technically straightforward anastomoses without leakage. However, achieving an inner diameter smaller than 100 µm proved challenging due to the limitation of the mold-based technique and the polymer shrinkage during the processing. Similar observations have been reported by other research groups, with the thickness of the TIPS layer cited as approximately 400 µm [34, 35]. This measurement exceeds the thickness of the TIPS layer reported in the present study.

Mesoscale morphology generally plays a critical role in graft performance, consistently in this study structural gradient produced a number of statistically significant effects. ES layers exhibited fiber diameters near 1 µm, a range previously associated with restricted cell infiltration, whereas the TIPS layer presented larger pores (30–100 µm) known to enhance migration and matrix deposition. Published reports indicate that the absences of a porous architecture can contribute to pathological conditions [36, 37] and may ultimately lead to the failure of the vascular device [38, 39]. Indeed, we found that differences in these design elements translated into distinct *in vivo* outcomes. ACR grafts maintained 100% patency at 4 and 8 weeks, whereas ICR grafts demonstrated occlusions in 2 rats for 8 weeks due to anastomotic intimal hyperplasia associated

with cell confinement within the bioactive and TIPS layers. These findings are in agreement with prior bilayer ES–TIPS systems in which spatially constrained bioactivity or limited pore continuity were associated with worse neointimal thickening [34]. The present data therefore reinforces the importance of tuning structural gradients across layers to selectively guide infiltration while avoiding excessive intimal hyperplasia.

The influence of the pore size, fibers diameter, microstructure and structural gradient has been investigated both *in vitro* and *in vivo* across various applications in the field of the tissue engineering [40-42]. Bergmeister et al. investigated *in vitro* and *in vivo* the cell infiltration and migration in polyurethane based TEVG fabricated by ES with different pore size (2 μm VS 4 μm) and porosity (53% VS 80%) [31]. *In vivo* analysis revealed that coarse mesh grafts (80% porosity) exhibited greater cell migration and long-term cell survival (up to 6 months) across all time points and regions of the conduit wall.
Tara et al. developed two distinct types of grafts: a large-pore graft composed of PLA fibers coated with PLCL, characterized by a pore size of approximately 30 μm, a porosity of 60%, and a fiber diameter of 20 μm, and a small-pore graft made from PLA nanofibers, featuring a pore size of around 0.7 μm, a porosity of 70%, and a fiber diameter of 0.7 μm [43]. The authors reported the presence of a well-organized neo-intima in the large-pore grafts. Furthermore, they noted, as in our study, that the high-density nanofiber scaffold exhibited a prolonged degradation rate, with minimal transmural cellular migration into the scaffold. Additionally, they corroborate that electrospun TEVG with fiber diameters less than 1 μm showed limited or no cellular infiltration. This result was previously demonstrated in literature [44] and it is aligned with the findings in this study.

To corroborate the concept of the structural gradient, in this study, that two occlusions were noted in the ICR groups at 8 weeks, both were attributed to intimal hyperplasia at the anastomosis. As previously discussed, the lumen of the graft is completely occluded due to the accumulation of collagen and cells that become confined within the bioactive layer and the intima TIPS layer, leading to over proliferation of the cells associated with intimal hyperplasia. Consistently, and with additional observations supporting the role of structural gradient on scaffold remodeling, the ACR group reported a higher number of VWF+/area cells at 8 weeks and a larger number of vasa vasorum at 4 weeks when compared to the ICR group. Specifically, the ACR and ICR groups exhibited a number of 38 ± 17 and of 13 ± 1 vasa vasorum, at 4 weeks, respectively. This observation has not been reported before and supports the remodeling towards of a more functional tunica adventitia. He et al. also reported in their study analogous phenomenon for poly(ester-urethane) urea bilayer grafts. In their design, the adventitia layer was generated through ES, while the intima layer was produced via TIPS [45].

The patency rate for the ACR group was 100% (9/9) at both 4 and 8 weeks, while the ICR group exhibited patency rates of 100% (8/8) at 4 weeks and 80% (8/10) at 8 weeks. This performance is superior to similar studies within the literature [24, 34].

Single layer VG made by polyurethane based material, for instance, demonstrated lower patency. A poly(ester urethane)urea (PEUU) ES VG (ID = 1.3 mm, thickness 150 μm) implanted in a rat model for 8 weeks, showed a patency of 40% [46]. Similarly, Nieponice et al. developed a cell-seeded PEUU ES-TIPS VG, which exhibited a patency rate of 65% at 8 weeks, in contrast to cell-

seeded PEUU TIPS (53%) and acellular PEUU TIPS (10%). Collectively, these findings suggest that both the chemical composition of the biomaterial and the morphology of the vascular graft significantly influence the early host response and function of the TEVG.

Other factors that significantly affect vivo function and remodeling include the size mismatch, the suture retention strength and the global compliance. From a surgical perspective, size matching is crucial for achieving successful anastomosis between the native vessel and the implanted graft, thereby restoring blood flow. The alignment of the shape and angle at the anastomotic junction facilitates blood flow restoration without causing excessive turbulence or a significant drop in hydraulic pressure. A size mismatch between the implant and the native vessel may create vortices or stagnant flow, both of which can reduce wall shear stress and potentially lead to graft occlusion over time. In this study, the dimensions of the grafts were adjusted to be as close as possible to the rat abdominal aorta. Inner diameter of the tested 3LVGs was comparable to the dimension of the rat abdominal aorta (**Table 1**). Although many studies have successfully tuned the mechanical properties of the TEVGs, only a limited number of studies report a simultaneous alignment of both thickness and compliance with the target vessel. The literature indicates that these grafts are often several hundred microns thicker than the rat aorta, which may limit cellular infiltration, and migration without recapitulating the structure and function of the native vessels. For example, Gao et al. tested electrospun amino acid-based poly(ester urea) small-diameter VGs with an ID approximately 1 mm, characterized by two distinct wall thickness: 250 μm and 350 μm [47].

The suture retention strength is a critical biomechanical characteristic that influences the performance of the graft immediately upon the release of the clamp to restore blood flow in vessel replacement. It is defined as the maximum force when the surgical wire is pulled out from the wall of the graft. This parameter is indicative of the challenges associated with suturing and the reliability of the suture connection during the implant. Indeed, the TEVGs should exhibit sufficient tensile and shear strength to endure the forces exerted by sutures throughout the grafting procedure [48]. This strength is essential to prevent rupture, early graft failure at the anastomosis and to mitigate local damage resulting from excessive loading at the suture sites [49].
In this study, the suture retention strength of the ACR and ICR 3LVG pre-implant was higher than that of the rat abdominal aorta. For the grafts, these values are similar to reported data for polyurethane-based VG designed for rat models [31, 50]. These experimental findings corroborated the performance of the graft during the surgical grafting procedure. Specifically, both ACR and ICR configurations were easy to suture onto the native rat aorta and effectively support the loads at the suture sites, demonstrating no bleeding at the anastomoses.

Considering that VGs should accommodate the vasodilatation and vasoconstriction of the native vessel, global compliance is an essential property to evaluate both pre-implantation and post-implantation. In this study, the global compliance preimplantation for the ACR and ICR configuration was significantly different in comparison to the rat abdominal aorta, in alignment with prior published reports. It has been repeatedly reported that polymeric VGs alone do not adequately replicate the elasticity of the native vessel due to the bulk stiffness of the biomaterial [19]. However, several studies have demonstrated the potential to tailor global compliance by altering the mesoscale structure of the graft. For instance, Bergmeister et al. investigated coarse-mesh and fine-mesh grafts, revealing that the coarse-mesh grafts exhibited significantly greater compliance (pre-implantation 7.2 ± 0.4% 100 mmHg) than fine-mesh grafts (pre-implantation 4.1

± 0.9% 100 mmHg) prior to implantation ($p<0.01$). Compliance decreased after implantation in the coarse-mesh graft (post-implantation 4.9 ± 0.4% 100 mmHg) and remained stable for the fine-mesh graft (3.9 ± 1.0% 100 mmHg). Additionally, Soletti et al. developed a conduit using the ES technique (fiber diameter approximately 1 μm) made from PEUU, onto which a non-thrombogenic copolymer was immobilized on the lumen [46]. Prior to implantation, the graft exhibited a lower compliance (5 ± 2 x 10^-4 mmHg^-1) compared to that of the native aorta (14 ± 1 x 10^-4 mmHg^-1). However, 4-weeks post-implantation, the compliance increased to levels comparable to those of native tissue.

In accordance with these results, this study demonstrates native-like compliance for the ACR configuration post-implantation at 8 weeks. while the ICR configuration post-implantation at 8 weeks remained significantly different in global compliance. This different remodeling outcome was attributed to the structural gradient, as the previous studies also stated. This was coupled to a more pronounced remodeling process in the ACR configuration compared to the ICR configuration at 8 weeks. As reported in (highlighting the middle portion of the explant), the ACR configuration at 4 and 8 weeks exhibited a surrogate-like structure due to the deposition of neo-ECM (H&E), collagen (MT), and elastin (VVG). In a pilot study, Nieponice et al. observed that a polyurethane-based ES graft can persist *in vivo* for more than 6 months without failing mechanically when implanted as a VG [34]. Additionally, they estimated that the TIPS layer can be sufficiently remodeled by that time, and the newly formed tissue will be strong enough to withstand systemic circulation. This balance between degradation and regeneration can facilitate effective remodeling and help prevent the formation of aneurysms or ruptures.
Therefore, the compliance of the implanted VG is a complex balance modulated by the morphology of the layers, the remodeling process and degradation rate *in vivo*. Ideally, matching the compliance of the vessel can provide a favorable mechanical environment for de novo ECM deposition [50, 51]. Eilenberg et al. developed a degradable polycarbonate urethane that was implanted into the infrarenal abdominal aorta of rat for 12 months [50].The compliance of the explanted graft improved after 12 months due to the structural thinning of the material from bulk degradation and the regeneration of new tissue.

Neo-intima formation and endothelization seems to occur within similar time windows. Bergmeister et al. observed *in vivo* rapid endothelial coverage of the luminal surfaces of both fine and coarse mesh grafts with, unlike in this study, no significant differences between the two fiber types [31]. In this particular case a dense protein layer promptly formed on the luminal surface, likely contributing to the observed lack of impact that variations in surface topography have on cellular colonization.

The need for a successful translational of small-diameter TEVGs also warrants further consideration. Symvess, the first FDA-approved acellular TEVG for extremity arterial repair, illustrates both the promise and current limitations of clinically available biologic conduits. Its off-the-shelf availability, avoidance of vein harvest, and encouraging short-term patency results have supported selective adoption. However, uncertainty regarding long-term durability, remodeling behavior, and cost-effectiveness has limited widespread replacement of autologous saphenous veins. Similarly to earlier generations of small-diameter ePTFE grafts that showed promising preclinical performance but later demonstrated significant clinical limitations related to thrombosis, compliance mismatch, and intimal hyperplasia [52]. These clinical observations

parallel experimental findings in the present work: while bioactive matrices support integration, they must be carefully spatially organized to avoid maladaptive hyperplasia. Multilayer constructs such as the 3LVG offer a potential avenue to reconcile the reproducibility of synthetic scaffolds with the regenerative capacity of biologic materials, most importantly the host cell recruitment route is a design variable for the next-generation TEVGs

While the current study highlights the importance of native blood vessel biomimicry to impact functional heterogeneity, some limitations must be acknowledged. First**,** while the use of rat abdominal replacement models offers significant advantages, such as cost-effectiveness and ease of surgical access, this model imperfectly recapitulates human hemodynamics, regenerative capacity, and vessel physiology. In particular, healthy rat models lack many clinically relevant features commonly observed in CABG and peripheral vascular patients, including chronic inflammation, hyperlipidemia, accelerated calcium-phosphate turnover, diabetes, and advanced atherosclerosis, all of which can influence graft remodeling and long-term patency. Future studies should consider larger animal models that more closely mimic human hemodynamics.
A second limitation, common to the vast majority of similar studies, was the length of the implanted 3LVGs. In CABG procedures, graft lengths typically exceed 20 cm. Therefore, the clinical assessment of shorter, small-diameter grafts might influence the patency and transanastomotic endothelialization as suggested by Skovrind et al. and Zilla et al. [53, 54].
Third, there were technical challenges in obtaining a TIPS intima layer thinner than 100 µm, which is necessary to match the thickness of the rat abdominal aorta. Scaling to a larger animal model may facilitate achieving the thickness and the mechanical compliance of native vessels.
Last, a fourth limitation should be considered: the absence of a commercially available synthetic graft as additional control group. However, currently available clinical grafts such as small-diameter ePTFE conduits are not manufactured at dimensions compatible with rat abdominal aortic implantation, making direct comparison technically challenging in this model. Nevertheless, future investigations in larger animal models could enable direct benchmarking against clinically established graft materials.

5. Conclusions

For patients with CAD, and more broadly for patients undergoing dialysis or affected by critical limb ischemia, the successful development of a small-diameter TEVG could reduce the need for repeated surgeries and lower the risk of complications associated with graft failure. This would not only enhance the quality of life for patients but also could reduce healthcare costs, given the ample spectrum of pathologies potentially addressed by an engineered vessel. Additionally, by alleviating the dependency on autologous vessels, this layered TEVG technology could expand the eligibility for surgical intervention, making life-saving treatments accessible to a broader patient's population.
The 3LVGs developed and characterized *in vitro* and assessed *in vivo* in this study, demonstrated good function and biomechanics, excellent patency rate (ACR configuration, 100% at 4 and 8 weeks) and scaffold remodeling, including endothelium formation, collagen elaboration and vasa vasorum formation.
Most importantly, this work established that biomimicry applied to native vessel functional heterogeneity via the concept of structural gradient can condition host cell infiltration, and scaffold remodeling ultimately leading to a higher patency rate. While the primary application remains the CABG procedure, the 3LVG design could potentially extend beyond small-diameter VG to address

various other biomedical applications, such as arteriovenous fistula for hemodialysis access, and grafts for treating critical limb ischemia. While this small animal pre-clinical study introduced and validated the general notion of structural biomimicry, follow-up research is needed to both discern molecular mechanisms and advance translational directions. In the future, conducting a longer-term study in rat models will elucidate remodeling mechanisms that may lead the ACR configuration to further develop a three-layer vessel surrogate. Finally, a size scale-up of the 3LVG device will be necessary to accommodate the functional and structural requirements of a larger animal model.

Acknowledgment
This work was financially supported by the Ri.MED Foundation "Dr. D'Amore' research support for years 2023-2024". The authors would like to acknowledge Dr. Neil Turner, Dr. Daniela Romero, and Mr. Nicholas Mosur for helping with immunofluorescence staining, Mr. Charles Patterson, Miss. Kelsey Hall, and Mr. Scott Johnson for providing assistance with the decellularization of the small intestine submucosa, and with the preparation of the SIS ECM, Dr. Ozeki for helping with the CT images, Dr. Simon Watkins, director of the Center for Biological Imaging, University of Pittsburgh, and Mr. Jonathan Franks for providing access and assistance to their advanced imaging facility, the Histology Laboratory managed by Julia Hart at the McGowan Institute for Regenerative Medicine of University of Pittsburgh for the histological staining, and the Division of Laboratory Animal Resources (DLAR) of University of Pittsburgh to support the small animal study. The authors would like to acknowledge Dr. Giuseppe D'Ancona who provided providing valuable clinical suggestions that helped improve the quality of the manuscript.

Conflict of interests
The authors declare the following financial interests/personal relationships which may be considered as potential competing interests: W.R. Wagner, A. D'Amore are inventors on patent #US12576192B2 issued to Ri.MED Foundation and University of Pittsburgh.

Data availability statement

All data supporting the findings of this study are included in the manuscript and its Supplementary Information. The datasets generated and/or analysed during the current study are available from the corresponding author upon reasonable request.

References

1. Martin, S.S., et al., *2024 Heart Disease and Stroke Statistics: A Report of US and Global Data From the American Heart Association.* Circulation, 2024. **149**(8): p. e347-e913.
2. Virani, S.S., et al., *Heart Disease and Stroke Statistics-2020 Update: A Report From the American Heart Association.* Circulation, 2020. **141**(9): p. e139-e596.
3. Tsao, C.W., et al., *Heart Disease and Stroke Statistics—2023 Update: A Report From the American Heart Association.* Circulation, 2023. **147**(8): p. e93-e621.
4. Libby, P., et al., *Atherosclerosis.* Nature Reviews Disease Primers, 2019. **5**(1): p. 56.
5. Zhang, F. and M.W. King, *Immunomodulation Strategies for the Successful Regeneration of a Tissue-Engineered Vascular Graft.* Advanced Healthcare Materials, 2022. **11**(12): p. 2200045.

6. Navab, M., et al., *The oxidation hypothesis of atherogenesis: the role of oxidized phospholipids and HDL.* J Lipid Res, 2004. **45**(6): p. 993-1007.
7. Libby, P., *The changing landscape of atherosclerosis.* Nature, 2021. **592**(7855): p. 524-533.
8. Neumann, F.-J., et al., *2018 ESC/EACTS Guidelines on myocardial revascularization.* European Heart Journal, 2018. **40**(2): p. 87-165.
9. Lawton, J.S., et al., *2021 ACC/AHA/SCAI Guideline for Coronary Artery Revascularization: A Report of the American College of Cardiology/American Heart Association Joint Committee on Clinical Practice Guidelines.* Circulation, 2022. **145**(3): p. e18-e114.
10. Zhang, Z., et al., *Vascugraft polyurethane arterial prosthesis as femoro-popliteal and femoro-peroneal bypasses in humans: pathological, structural and chemical analyses of four excised grafts.* Biomaterials, 1997. **18**(2): p. 113-24.
11. Panagiotopoulos, I., et al., *The choice of conduits in coronary artery bypass surgery.* Arch Med Sci Atheroscler Dis, 2023. **8**: p. e83-e88.
12. Beerkens, F.J., et al., *Contemporary coronary artery bypass graft surgery and subsequent percutaneous revascularization.* Nature Reviews Cardiology, 2022. **19**(3): p. 195-208.
13. Alexander, J.H. and P.K. Smith, *Coronary-Artery Bypass Grafting.* New England Journal of Medicine, 2016. **374**(20): p. 1954-1964.
14. Escaned, J., *Secondary revascularization after CABG surgery.* Nature Reviews Cardiology, 2012. **9**(9): p. 540-549.
15. Goldman, S., et al., *Long-term patency of saphenous vein and left internal mammary artery grafts after coronary artery bypass surgery: Results from a Department of Veterans Affairs Cooperative Study.* Journal of the American College of Cardiology, 2004. **44**(11): p. 2149-2156.
16. Seifu, D.G., et al., *Small-diameter vascular tissue engineering.* Nat Rev Cardiol, 2013. **10**(7): p. 410-21.
17. Chang, H.W., H.J. Han, and K.H. Park, *Long-term patency of bilateral internal thoracic artery Y composite coronary artery bypass grafts-determinants and impact on survival.* J Thorac Dis, 2022. **14**(6): p. 1909-1921.
18. Kannan, R.Y., et al., *Current status of prosthetic bypass grafts: a review.* Journal of Biomedical Materials Research Part B: Applied Biomaterials: An Official Journal of The Society for Biomaterials, The Japanese Society for Biomaterials, and The Australian Society for Biomaterials and the Korean Society for Biomaterials, 2005. **74**(1): p. 570-581.
19. Pashneh-Tala, S., S. MacNeil, and F. Claeyssens, *The tissue-engineered vascular graft—past, present, and future.* Tissue Engineering Part B: Reviews, 2016. **22**(1): p. 68-100.
20. Hoenig, M.R., et al., *Tissue-Engineered Blood Vessels: Alternative to Autologous Grafts?* Arteriosclerosis, Thrombosis, and Vascular Biology, 2005. **25**(6): p. 1128-1134.
21. Wang, X., et al., *Development of Small-Diameter Vascular Grafts.* World Journal of Surgery, 2007. **31**(4): p. 36.
22. Xie, X., et al., *Five types of polyurethane vascular grafts in dogs: the importance of structural design and material selection.* J Biomater Sci Polym Ed, 2010. **21**(8-9): p. 1239-64.
23. Curi, M.A., et al., *Long-term safety and efficacy outcomes of the Acellular Tissue Engineered Vessel (ATEV) in extremity arterial trauma repair.* J Vasc Surg Cases Innov Tech, 2026. **12**(1): p. 102042.
24. Koch, S.E., et al., *Animal studies for the evaluation of in situ tissue-engineered vascular grafts — a systematic review, evidence map, and meta-analysis.* npj Regenerative Medicine, 2022. **7**(1): p. 17.
25. Ibrahim, D.M., et al., *Functional regeneration at the blood-biomaterial interface.* Advanced Drug Delivery Reviews, 2023. **201**: p. 115085.

26. Gu, X., et al., *Biodegradable, elastomeric coatings with controlled anti-proliferative agent release for magnesium-based cardiovascular stents.* Colloids and Surfaces B: Biointerfaces, 2016. **144**: p. 170-179.
27. Hong, Y., et al., *Tailoring the degradation kinetics of poly(ester carbonate urethane)urea thermoplastic elastomers for tissue engineering scaffolds.* Biomaterials, 2010. **31**(15): p. 4249-4258.
28. Hussey, G.S., et al., *Ultrasonic cavitation to prepare ECM hydrogels.* Acta Biomaterialia, 2020. **108**: p. 77-86.
29. Ye, S.-H., et al., *Nonthrombogenic, Biodegradable Elastomeric Polyurethanes with Variable Sulfobetaine Content.* ACS Applied Materials & Interfaces, 2014. **6**(24): p. 22796-22806.
30. Hong, Y., et al., *A small diameter, fibrous vascular conduit generated from a poly(ester urethane)urea and phospholipid polymer blend.* Biomaterials, 2009. **30**(13): p. 2457-2467.
31. Bergmeister, H., et al., *Healing characteristics of electrospun polyurethane grafts with various porosities.* Acta Biomaterialia, 2013. **9**(4): p. 6032-6040.
32. Gong, W., et al., *Hybrid small-diameter vascular grafts: Anti-expansion effect of electrospun poly ε-caprolactone on heparin-coated decellularized matrices.* Biomaterials, 2016. **76**: p. 359-370.
33. Adamo, A., et al., *Continuous Microfiber Wire Mandrel-Less Biofabrication for Soft Tissue Engineering Applications.* Advanced Healthcare Materials, 2022. **11**(13): p. 2102613.
34. Nieponice, A., et al., *In Vivo Assessment of a Tissue-Engineered Vascular Graft Combining a Biodegradable Elastomeric Scaffold and Muscle-Derived Stem Cells in a Rat Model.* Tissue Engineering Part A, 2009. **16**(4): p. 1215-1223.
35. Krawiec, J.T., et al., *In Vivo Functional Evaluation of Tissue-Engineered Vascular Grafts Fabricated Using Human Adipose-Derived Stem Cells from High Cardiovascular Risk Populations.* Tissue Engineering Part A, 2016. **22**(9-10): p. 765-775.
36. Stenmark, K.R., et al., *The adventitia: essential regulator of vascular wall structure and function.* Annu Rev Physiol, 2013. **75**: p. 23-47.
37. Marziano, C., G. Genet, and K.K. Hirschi, *Vascular endothelial cell specification in health and disease.* Angiogenesis, 2021. **24**(2): p. 213-236.
38. Ratner, B., *Vascular Grafts: Technology Success/Technology Failure.* BME Frontiers, 2023. **4**: p. 0003.
39. Mehta, R.I., et al., *Pathology of explanted polytetrafluoroethylene vascular grafts.* Cardiovascular Pathology, 2011. **20**(4): p. 213-221.
40. Karageorgiou, V. and D. Kaplan, *Porosity of 3D biomaterial scaffolds and osteogenesis.* Biomaterials, 2005. **26**(27): p. 5474-5491.
41. Zonderland, J., et al., *Fiber diameter, porosity and functional group gradients in electrospun scaffolds.* Biomedical Materials, 2020. **15**(4): p. 045020.
42. Lowery, J.L., N. Datta, and G.C. Rutledge, *Effect of fiber diameter, pore size and seeding method on growth of human dermal fibroblasts in electrospun poly(ε-caprolactone) fibrous mats.* Biomaterials, 2010. **31**(3): p. 491-504.
43. Tara, S., et al., *Well-organized neointima of large-pore poly(l-lactic acid) vascular graft coated with poly(l-lactic-co-ε-caprolactone) prevents calcific deposition compared to small-pore electrospun poly(l-lactic acid) graft in a mouse aortic implantation model.* Atherosclerosis, 2014. **237**(2): p. 684-691.
44. Rocco, K.A., et al., *In Vivo Applications of Electrospun Tissue-Engineered Vascular Grafts: A Review.* Tissue Engineering Part B: Reviews, 2014. **20**(6): p. 628-640.
45. He, W., et al., *Pericyte-based human tissue engineered vascular grafts.* Biomaterials, 2010. **31**(32): p. 8235-8244.

46. Soletti, L., et al., *In vivo performance of a phospholipid-coated bioerodable elastomeric graft for small-diameter vascular applications.* Journal of Biomedical Materials Research Part A, 2011. **96A**(2): p. 436-448.
47. Gao, Y., et al., *Pilot Mouse Study of 1 mm Inner Diameter (ID) Vascular Graft Using Electrospun Poly(ester urea) Nanofibers.* Adv Healthc Mater, 2016. **5**(18): p. 2427-36.
48. Meng, X., et al., *Suture retention strength of P(LLA-CL) tissue-engineered vascular grafts.* RSC Adv, 2019. **9**(37): p. 21258-21264.
49. Pensalfini, M., et al., *The suture retention test, revisited and revised.* Journal of the Mechanical Behavior of Biomedical Materials, 2018. **77**: p. 711-717.
50. Eilenberg, M., et al., *Long Term Evaluation of Nanofibrous, Bioabsorbable Polycarbonate Urethane Grafts for Small Diameter Vessel Replacement in Rodents.* European Journal of Vascular and Endovascular Surgery, 2020. **59**(4): p. 643-652.
51. Zhu, M., et al., *Biodegradable and elastomeric vascular grafts enable vascular remodeling.* Biomaterials, 2018. **183**: p. 306-318.
52. Hernandez-Sanchez, D., et al., *Manufacturing and validation of small-diameter vascular grafts: A mini review.* iScience, 2024. **27**(6): p. 109845.
53. Skovrind, I., et al., *Concise Review: Patency of Small-Diameter Tissue-Engineered Vascular Grafts: A Meta-Analysis of Preclinical Trials.* Stem Cells Transl Med, 2019. **8**(7): p. 671-680.
54. Zilla, P., D. Bezuidenhout, and P. Human, *Prosthetic vascular grafts: wrong models, wrong questions and no healing.* Biomaterials, 2007. **28**(34): p. 5009-27.